International Immunopharmacology 77 (2019) 105968

Contents lists available at ScienceDirect

International Immunopharmacology

journal homepage: www.elsevier.com/locate/intimp

Tanshinone IIA ameliorates the bleomycin-induced endothelial-to-mesenchymal transition via the Akt/mTOR/p70S6K pathway in a murine model of systemic sclerosis

Ying Jiang[a,1], Feifei Hu[a,1], Qiao Li[b,1], Chen Shen[a], Ji Yang[a], Ming Li[a,*]

[a] Department of Dermatology, Zhongshan Hospital, Fudan University, 180 Fenglin Road, Shanghai 200032, China
[b] Department of Dermatology, Huashan Hospital, Fudan University, Shanghai, China

ARTICLE INFO

Keywords:
Systemic sclerosis
Endothelial-to-mesenchymal transition
Tanshinone IIA
Bleomycin

ABSTRACT

Systemic sclerosis (SSc) is an autoimmune inflammatory and vascular disorder leading to progressive tissue fibrosis. Tanshinone IIA (Tan IIA) is a phytochemical extracted from the Chinese herb *Salvia miltiorrhiza* that exhibits diverse activities. In this study, we attempted to evaluate the potential impact of Tan IIA on the skin fibrosis-related endothelial-to-mesenchymal transition (EndoMT) and investigate the underlying molecular mechanisms. EndoMT-related indexes including morphological characteristics, functional changes, histological parameters, expression levels of extracellular matrix associated genes, and changes in the expression of related biomarkers in dermal fibrosis were assessed. Tan IIA had a strong anti-fibrotic effect through amelioration of skin thickness and collagen deposition. Moreover, Tan IIA partially reversed bleomycin-induced EndoMT both *in vivo* and *in vitro*. Additionally, Tan IIA mitigated the diminution of tube formation in endothelial cells induced by bleomycin. Furthermore, mechanistically, the activation of the Akt/mTOR/p70S6K pathway was found to be involved in bleomycin-treated SSc mouse model, which was alleviated by Tan IIA. In summary, these data suggest that Tan IIA alleviates SSc-related dermal fibrosis and EndoMT and that the Akt/mTOR/p70S6K signaling pathway is involved in this regulation, thus supporting the potential of Tan IIA as a disease-modifying candidate agent for treating the vascular damage of SSc.

1. Introduction

Systemic sclerosis (SSc) is a multisystem autoimmune connective tissue disease characterized by widespread microangiopathy, disordered immunity, and excessive fibrosis of various organs [1,2]. Although its exact pathogenesis still remains elusive, it is generally recognized and accepted that the injury of vascular endothelial cells plays an important role in the vascular remodeling observed in SSc patients [3]. Endothelial cells in patients with SSc are damaged or aberrantly activated, leading to abnormal structural and functional changes, such as destructive, proliferative, and obliterative vasculopathy, which eventually results in tissue fibrosis [4].

Recently, several studies have shown that the impaired functional activation of the SSc vasculature results from the activation of the endothelial-to-mesenchymal transition (EndoMT) [5,6]. EndoMT is a complex progress by which endothelial cells lose polarities, turn into a myofibroblastic or mesenchymal phenotype, lose intrinsic endothelial biomarkers, and express mesenchymal biomarkers [7]. Transforming growth factor-β (TGF-β)-induced EndoMT is involved in the pathogenesis of vasculopathy in SSc [8,9]. In fact, two types of transcriptional regulators are implicated in the regulation of EndoMT; namely the zinc-finger binding factors like Snail1 and Slug (also known as Snail2) and the basic helix-loop-helix factors like Twist [10–12]. During the process of bleomycin-induced EndoMT in endothelial cells, the Akt/mammalian targets of the rapamycin (mTOR) signal pathway [13,14] and the TGF-β/Smad signal pathway [15] are both involved. Furthermore, several studies have pointed out that mTOR signal pathway also takes part in TGF-β_1-induced EndoMT [16] and the TGF-β_2-induced epithelial-mesenchymal transition (EMT) [17].

Tanshinone IIA (Tan IIA; $C_{19}H_{18}O_3$; PubChem CID: 164676; 14,16-epoxy-20-nor-5(10),6,8,13,15-abietapentaene-11,12-dione) is an active diterpene quinone of *Salvia miltiorrhiza* Bunge [18], which is a well-known traditional Chinese herbal medicine used to relieve vessel stasis and promote blood circulation [19]. Recent studies have further

* Corresponding author.
E-mail address: li.ming@zs-hospital.sh.cn (M. Li).
[1] Contributed equally.

https://doi.org/10.1016/j.intimp.2019.105968
Received 4 June 2019; Received in revised form 5 October 2019; Accepted 7 October 2019
Available online 06 November 2019
1567-5769/ © 2019 Published by Elsevier B.V.

revealed that tanshinones are particularly relevant for their antitumor [20], antioxidant [21], and anti-inflammatory properties [22]. Notably, Tan IIA, the main active ingredient in tanshinone, exhibits multiple desirable features such as the downregulation of expression of various inflammatory cytokines [23], alleviation of ischemia/reperfusion-induced injury [24], amelioration of hypoxia-induced EndoMT [25], and exertion of protective effects in pulmonary, cardiac, renal, and hepatic fibrosis [26–30]. Furthermore, Tan IIA can modulate inflammation in several autoimmune disorders such as SSc [31] and systemic lupus erythematosus [32]. In addition, Tan IIA can reduce pulmonary artery pressure and mitigate hypoxia-induced pulmonary artery remodeling [33]. However, the mechanisms underlying the Tan IIA-mediated anti-fibrotic effects are still poorly understood. Therefore, we conducted both *in vitro* and *in vivo* studies to investigate the effects of Tan IIA on SSc-related EndoMT and dermal fibrosis and to further elucidate the molecular mechanisms underlying its anti-fibrotic activity.

2. Materials and methods

2.1. Reagents and antibodies

Tan IIA (99.0% pure) was obtained from the Boyun Biotech Company (Shanghai, China), rapamycin (RAP) was purchased from Sigma-Aldrich (St. Louis, MO, USA), and bleomycin (BLM) was acquired from Nippon Kayaku (Tokyo, Japan). Tan IIA was dissolved as a 10 mg/mL stock solution in dimethylsulfoxide (DMSO; Sigma-Aldrich, USA) and stored in the dark at −20 °C. Culture media and buffers were purchased from Promocell (Heidelberg, Germany). The primary antibodies described in this article include anti-Akt, anti-phosphorylated Akt (Ser473), anti-mTOR, anti-phosphorylated mTOR(Ser2448), anti-p70 S6 kinase, anti-phosphorylated p70 S6 kinase (Thr389), anti-Slug, anti-GAPDH, and β-actin (Cell Signaling Technology, CA, USA); anti-collagen III, anti-collagen I, anti-α smooth muscle actin (α-SMA), anti-CD31, anti-vascular endothelial (VE)-cadherin, anti-Twist, anti-Snail, and anti-fibroblast specific protein-1 (FSP1)/S100A4 (Abcam, New York, USA). Other materials and chemicals were purchased from the KeyGEN Biotechnology Company or Beyotime Institute of Biotechnology (Nanjing, China) unless otherwise indicated.

2.2. Establishment of skin fibrosis mouse model

Female C57BL/6 mice (n = 48), aged 7 weeks and weighing 20–22 g, were purchased from the Vitalriver Laboratory Animal Center (Beijing, China). Mice were randomly assigned to one of four groups: Control, BLM, Tan IIA, or rapamycin. Bleomycin was dissolved in saline at a concentration of 500 μg/mL and then sterilized by filtration. In the BLM, Tan IIA, and rapamycin groups, BLM (100 μL/day) was injected subcutaneously into a single location on the shaved backs of the mice with a 27-gauge needle, while the mice received the same volume of saline in the control group. Tan IIA (10 mg/kg body weight), rapamycin (1.5 mg/kg body weight), or the vehicle was administered intraperitoneally together with s.c. bleomycin or saline. Prolonged administration of Tan IIA (10 mg/kg) or rapamycin (1.5 mg/kg) for up to 21 d was well tolerated with no signs of toxicity observed. Rapamycin was used as a positive control for mTOR inhibition because previous studies have shown that it is implicated in both the BLM-induced SSc mouse model [34] and EndoMT in human umbilical vein endothelial cells (HUVECs) [13]. Mice were anesthetized and sacrificed on day 21 after the initial BLM injection. Skin tissues were fixed in 4% paraformaldehyde and dehydrated. They were then embedded in paraffin for histological analysis or molecular experiments. All animal experimental procedures were in strict line with the relevant regulations and guidelines. All methods were approved by the Animal Care and Use Committee of Zhongshan Hospital, Fudan University (Shanghai, China).

2.3. Cell culture and treatment

HUVECs (Promocell, Heidelberg, Germany) were cultured in endothelial cell growth medium maintained at 37 °C in a humidified 5% CO_2 atmosphere. Cells were used in passages 2–7. HUVECs were detached with 0.25% trypsinization (Promocell) and seeded into 6-well plates at a density of 1×10^5 cells per well. HUVECs with a confluence of 70–80% were pre-stimulated with 10 μg/mL Tan IIA, rapamycin (200 nM), or control DMSO (final concentration of less than 0.05% as a vehicle) for 2 h before BLM (2 μg/mL) treatment. After an additional 48 h treatment, the cells were analyzed for protein expression. Furthermore, the HUVECs were incubated with different dosages of Tan IIA (5, 10, and 15 μg/mL) for 2 h, respectively, in the presence of BLM (2 μg/mL). The following morphological examination and western blot analysis were then performed on these HUVECs.

2.4. Morphological analysis and tube formation assay

HUVECs were treated with Tan IIA (10 μg/mL), rapamycin (200 nM), or control DMSO for 2 h in the presence and absence of BLM (2 μg/mL). An inverted microscope (Leica, Germany) was used to observe the cell morphology. We randomly captured digital images of the HUVECs and examined the morphologic characteristics at 40x magnification. Briefly, aliquots of Matrigel (150 μL; Corning) were added into a 48-well plate and then incubated at 37 °C for 30 min. HUVECs were pretreated as follows: (1) vehicle + vehicle, (2) vehicle + BLM, (3) Tan IIA + BLM, or (4) rapamycin + BLM. Cells were then seeded onto the gel at a density of 2×10^4 cells per well. After 6 h incubation in a humidified incubator (37 °C, 5% CO_2), five random fields were selected from each well and photographed. Image Pro Plus software 6.0 (Media Cybernetic, Silver Spring, Mass., USA) was used to measure the networks of tube-like structures.

2.5. Histological analysis

All skin sections were stained using hematoxylin and eosin (H&E) staining, Masson's trichrome staining, and immunohistochemical staining to investigate the severity of skin fibrosis and collagen deposition. We measured the dermal thickness, which was defined as the thickness from the dermal-epidermal junction to the dermal-subcutaneous fat junction [35]. To ensure the homogeneous and representative of histological data, we counted five randomly selected independent microscopic fields per specimen. Two independent examiners (Y.J. and FF.H.) evaluated and assessed the results using a Nikon Eclipse 80i microscope (Nikon, Badhoevedorp, Netherlands). Next, the distribution and degree of expression of α-SMA, CD31, and Slug in the skin tissues was determined by immunohistochemical staining. Briefly, paraffin sections were dewaxed and rehydrated using xylene and various concentrations of ethanol. After microwave antigen retrieval, H_2O_2 quenching and blocking were performed with 5% bovine serum albumin at room temperature. Then, primary antibodies for CD31 (1:100), Slug (1:50), and α-SMA (1:100) were applied to the slides, followed closely by incubation at 4 °C overnight. Horseradish peroxidase-conjugated goat anti-rabbit IgG secondary antibody was applied to incubate the slides at 37 °C for 1 h. The nucleus was then counterstained with Harris hematoxylin. A microscope equipped with a digital camera (Leica, Germany) was used to acquire all the images.

2.6. Immunofluorescence

After antigen retrieval, quenching of auto-fluorescence, and blocking of nonspecific binding sites [6], the skin sections (5 μm thick) were examined by double-label immunofluorescence using antibodies against CD31 (1:50) and α-SMA (1:100), followed by fluorochrome-conjugated secondary antibodies (Cell Signaling Technology) and DAPI to verify the nuclei. In order to confirm specificity, negative controls

were stained without primary antibodies. CD31 and α-SMA exhibited red and green fluorescence, respectively. All of the images were captured using fluorescence microscopy (Olympus BX51W1, Tokyo, Japan). The proportion of vessels with CD31/α-SMA co-localization was scored in at least six randomly selected high-power fields from each mouse by two independent examiners (Y.J. and FF.H.) in a blinded fashion as mentioned previously.

2.7. RNA extraction and real-time RT-PCR

Total RNA of HUVECs and skin tissues was extracted and purified with Trizol reagent (Invitrogen, Carlsbad, CA, USA) following the protocol provided by the manufacturer. Next, cDNA was synthesized using a PrimeScript™ RT reagent kit (TaKaRa Biotechnology, Shiga, Japan). Real-time PCR samples were prepared with SYBR Premix Ex Taq (TakaRa Biotech, Tokyo, Japan) using an ABI Prism 7900 Detector System (Applied Biosystems). Real-time PCR was performed using the method described previously [34]. The specific primers used for PCR were as follows: Collagen 1a1 (Col1a1), F: 5′-GCTCCTCTTAGGGGCC ACT-3′ and R: 5′-ATTGGGGACCCTTAGGCCAT-3′; Collagen 1a2 (Col1a2), F: 5′-AAGGGTGCTACTGGACTCCC-3′ and R: 5′-TTGTTACCG GATTCTCCTTTGG-3′; α-SMA, F: 5′- CCCAGACATCAGGGAGTAA TGG-3′ and R: 5′-TCTATCGGATACTTCAGCGTCA-3′; CD31, F: 5′-ACG CTGGTGCTCTATGCAAG-3′ and R: 5′-TCAGTTGCTGCCCATTCATCA-3′; GAPDH, F: 5′-AGGTCGGTGTGAACGGATTTG-3′ and R: 5′-GGGGTCGT TGATGGCAACA-3′. The expression levels were normalized to the GAPDH gene by using the $2-^{\triangle\triangle Ct}$ method.

2.8. Western blotting

HUVECs or skin tissues were lysed in ice-cold RIPA Lysis Buffer supplemented with protease inhibitor. Protein concentrations of the lysate were measured with a BCA protein assay kit, and equal amounts of protein (40 μg) were loaded on a 10% sodium dodecyl sulfate polyacrylamide gel for electrophoresis and transferred to PVDF membrane (Millipore, Germany). After blocking with 5% skimmed milk or Tris-buffered saline with Tween 20 (TBST) solution containing 5% bovine serum albumin for 2 h followed by TBST washing four times, membranes were incubated with primary antibodies overnight at 4 °C. We washed the membrane with TBST four times. The membrane was incubated with the appropriate secondary antibodies for 2 h at room temperature and detected with ECL reagents (Pierce). Selected blots were quantified using Image J (NIH, USA).

2.9. Statistical analysis

The results are presented as means ± standard deviation values. All of the analyses were performed using GraphPad Prism software (Graphpad Software, La Jolla, CA, USA). A value of $p < 0.05$ was considered statistically significant.

3. Results

3.1. Tan IIA ameliorated dermal fibrosis in the bleomycin-induced SSc mouse model

As the H&E and Masson's trichrome staining revealed, the BLM treatment showed an apparent increase in dermal thickening as well as in skin collagen content compared with the control (Fig. 1A, B), while Tan IIA or rapamycin treatment significantly attenuated the dermal thickness and downregulated the collagen content (Fig. 1C, E). Furthermore, a BLM-dependent decrease in the dermal white adipose tissue layer, which is generally seen in mice administered with BLM [36], was noticeably augmented by Tan IIA treatment (Fig. 1D). Additionally, to investigate the impact of Tan IIA on the production of ECM, we explored the transcription levels of the Col1a1 and Col1a2 genes. Relative expression of these genes was apparently decreased in BLM-treated mice exposed to Tan IIA or rapamycin than in those without Tan IIA or rapamycin administration, as shown in Fig. 1F.

3.2. Tan IIA alleviated EndoMT induced by BLM in HUVECs

Continuous treatment with BLM for 48 h caused dramatic changes *in vitro*. Cell morphology was transformed from a cobblestone-like shape into an elongated, spindle-shaped fibroblast-like appearance. This transformation was ameliorated by Tan IIA or rapamycin treatment (Fig. 2A). Meanwhile, HUVECs in the PBS- (control-) treated group did not induce a transformation in EndoMT-associated cell shape. Additionally, western blotting results confirmed a decreased expression of endothelial biomarkers (CD31 and VE-cadherin) and elevated levels of mesenchymal cell biomarkers, including α-SMA, FSP-1, collagen I, and collagen III, as compared with their levels in control (Fig. 2B and C). Correspondingly, western blot analysis revealed that BLM reduced expression of endothelial biomarkers, which could be resisted by treatment with Tan IIA or rapamycin. Furthermore, compared with the control group, overexpression of α-SMA and FSP1 proteins induced by BLM could also be inverted by Tan IIA or rapamycin (Fig. 2C). Moreover, there was no statistically significant difference in expression of endothelial markers between the BLM + rapamycin and the BLM + Tan IIA groups.

3.3. Tan IIA reversed EndoMT in a dose-dependent manner

BLM significantly downregulated the expression of CD31 and upregulated the protein level of α-SMA. Notably, such results were reversed by Tan IIA in a dose-dependent manner (Fig. 2D).

3.4. Tan IIA restored tube formation impaired by BLM

After 6 h of BLM incubation with exposure to Tan IIA or rapamycin, cell formation was photographed under inverted microscopy. Treatment of Tan IIA and rapamycin significantly restored tube formation destroyed by BLM as compared with the response in the BLM-treated group (Fig. 3A).

3.5. Tan IIA attenuated the EndoMT in the SSc mouse model

In the control group, α-SMA expression in the dermal microvasculature was mostly restricted to vascular smooth muscle cells and pericytes, as expected [6]. In contrast, we observed the co-localized CD31/α-SMA in the endothelium of dermal capillary vessels and numerous arterioles in murine skin, which indicated the intermediate stages of EndoMT (Fig. 4A). As displayed in Fig. 4B, using these two markers in combination, we observed that the transitional EndoMT was present at a rather low level in the control, while in the BLM-treated group, the level of transitional EndoMT was significantly higher ($p < 0.05$). Additionally, this elevated percentage of double-positive cells in the BLM-treated group could also be inverted in the dermis of SSc mice treated with Tan IIA or rapamycin (Fig. 4B).

We performed further immunohistochemistry analysis, by staining the samples with the primary antibodies for α-SMA and CD31. As shown in Fig. 5, CD31 was expressed continuously at the intima of the capillary vessels in the control group, while the continuous expression of CD31 (Fig. 5B) was damaged and displaced by elevated levels of α-SMA (Fig. 5B) surrounding the capillary vessels in most of the mice treated with BLM. Some even invaded the endothelial cell layers. Indeed, the number of cells positive for α-SMA was increased and CD31 was decreased in SSc mice compared with that in the control. Similarly, these changes could also be resisted by Tan IIA or rapamycin treatment.

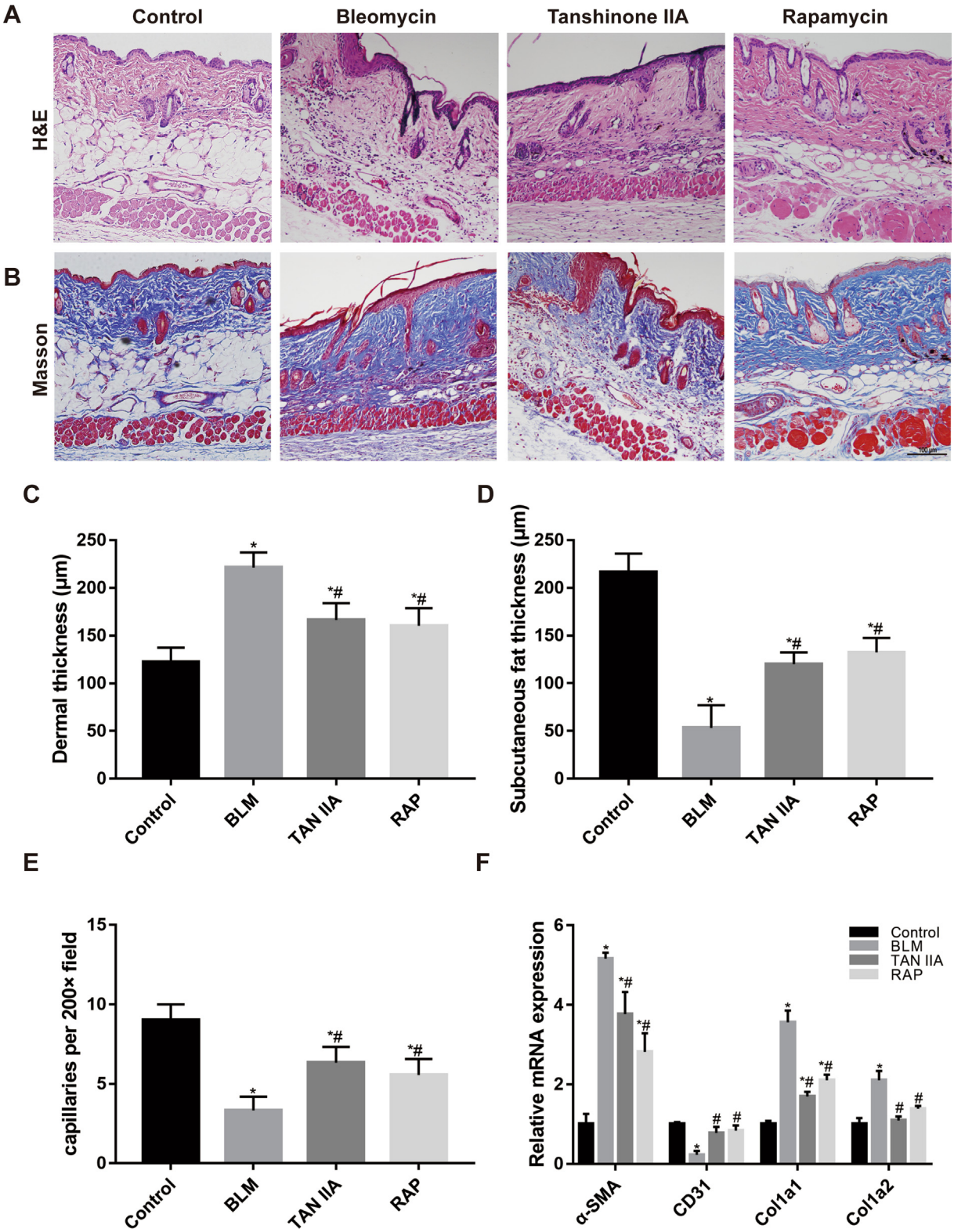

Fig. 1. Tanshinone IIA ameliorated dermal fibrosis in a BLM-induced mouse model. Representative images of hematoxylin and eosin (H&E) staining (A) and Masson trichrome staining (B) results. The original magnification is 100x. (C) Dermal thickness was calculated at 200x microscopic magnification, as indicated by H&E staining. (D) Data on subcutaneous fat thickness are summarized as a histogram. (E) Computerized histogram analysis of the capillaries. (F) ECM-related gene expression in the mouse skin was detected by real-time PCR, and mRNA levels were calculated using their ratios relative to GAPDH. Each graph indicates the mean ± standard error of the mean of the indicated parameters (n = 6–7 per group). Scale bars = 100 μm for A and B. $^{*}p < 0.05$ versus the control group; $^{\#}p < 0.05$ versus the BLM group.

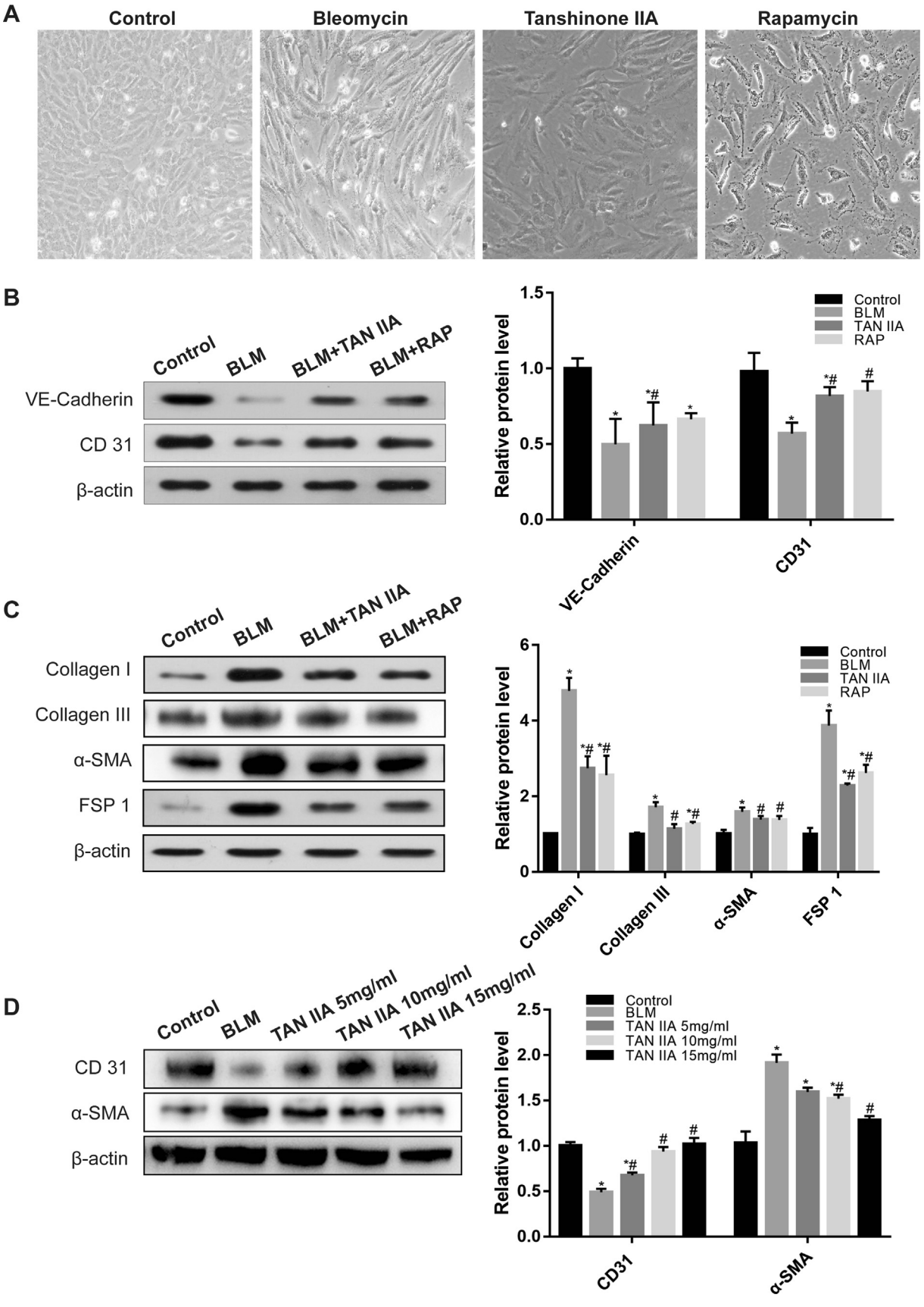

(caption on next page)

Fig. 2. Tanshinone IIA ameliorated EndoMT induced by BLM in HUVECs. (A) Confluent HUVECs were stimulated with PBS + control dimethylsulfoxide, BLM + control dimethylsulfoxide, BLM + tanshinone IIA, or BLM + rapamycin under identical conditions. After 48 h of stimulation, the cell morphology was observed under the microscope. Effects of tanshinone IIA on the expression of endothelial (B) and mesenchymal (C) cell biomarkers in HUVECs treated with BLM. Western blot results and the histogram depict the relative protein level in each group. (D) Tanshinone IIA reversed BLM-induced EndoMT-related protein levels in HUVECs in a dose-dependent manner. The protein levels of CD31 and α-SMA were detected by western blot. All of the figures are from one representative out of more than three similar experiments. $^{*}p < 0.05$ versus the control group; $^{\#}p < 0.05$ versus the BLM group.

3.6. Tan IIA inhibited the transcriptional factor Slug in BLM-induced EndoMT

Considering the important roles of transcription factors in EndoMT [37], we measured their protein levels and found that those of Slug, Snail, and Twist were significantly increased in the BLM group as compared with the control (Fig. 6). Treatment with Tan IIA or rapamycin for 48 h reversed BLM-induced Slug and Twist expression, while the difference between the BLM + Tan IIA and BLM + rapamycin groups was not statistically significant. Furthermore, compared to the control group, the immunohistochemistry analysis showed an increased number of Slug-positive endothelial cells in the BLM group (Fig. 6C), and this upregulation was significantly reduced in the BLM + Tan IIA and BLM + rapamycin groups.

3.7. Tan IIA inhibited the Akt/mTOR/p70S6K pathway in the SSc mouse model

Since several EndoMT-related transcription factors could be regulated by the Akt pathway [13,38], including Slug and Snail, we explored the activation of the Akt/mTOR/p70S6K pathway and found that the phosphorylation of Akt and the downstream factors mTOR and p70S6K were strongly apparent in the BLM mice, which could also be ameliorated by Tan IIA or rapamycin (Fig. 7). In our experiments, after using rapamycin, the mTOR inhibitor BLM failed to transform endothelial cells (Fig. 2A), and this was later confirmed by immunofluorescence analysis (Fig. 4). Furthermore, it was observed that the diminished tube formation was significantly restored by Tan IIA or rapamycin (Fig. 3).

4. Discussions

In view of the mild and broad therapeutic effects of *Salvia miltiorrhiza* in modulating a wide range of molecular activities implicated in the pathogenesis of SSc, we sought to evaluate the impact of Tan IIA, the principal constituent of *Salvia miltiorrhiza*, in the bleomycin-treated mice model. The present study employed both *in vivo* and *in vitro* experiments to explore the efficacy of Tan IIA and rapamycin on bleomycin-induced EndoMT along with their potential mechanisms. We found that Tan IIA treatment suppressed bleomycin-mediated murine dermal fibrosis by ameliorating the activation of fibroblasts and EndoMT. Importantly, Tan IIA moderated experimental skin fibrosis both *in vivo* and *in vitro*. Furthermore, this anti-EndoMT impact was mediated at least partially by inhibition of the Akt/mTOR/p70S6K signaling pathway.

Fibrosis is the major clinical feature of SSc, and is caused by a switch of the tissue fibroblasts into an active state with the synthesis of excessive ECM. The vascular damage and subsequent vascular response are thought to be present before and lead to collagen deposition. Some even argue that the vascular involvement can represent the main onset of SSc [39]. To better understand the underlying mechanism by which injury to the microvascular and macrovascular system contributes to fibrosis, various hypotheses have been put forward. A highly interesting development in this field suggests that EndoMT is another possible source of tissue myofibroblasts, and that this transdifferentiation might be a significant source of the mesenchymal cells involved in the fibroproliferative vasculopathy and tissue fibrosis in SSc [8,40]. In fact, EndoMT could explain how the persistence of vascular-fibroblast crosstalk can be considered a pro-fibrotic loop-promoting situation in SSc.

In the present study, we explored the anti-fibrotic effects of Tan IIA and its mechanism, noting first that Tan IIA alleviated experimental dermal fibrosis in the mouse model of SSc, which further confirmed its therapeutic effect. At the same time, we observed a protective switch from induced endothelial to mesenchymal forms by Tan IIA, as recently described in the literature [15,41]. We found that this protective effect of EndoMT could be reversed by Tan IIA in a dose-dependent manner. As already mentioned, Tan IIA has traditionally been used clinically in treating patients with pulmonary fibrosis [27] and liver fibrosis [29,42]. In addition, further evidence indicates that Tan IIA administration notably inhibits BLM-triggered abnormal collagen deposition, reverses TGF-β_1-stimulated EndoMT, and suppresses TGF-β/Smad signal transduction in the lungs induced by BLM [15]. Our previous studies also indicated that Tan IIA exerts an inhibitory influence on the functional activation of SSc patient-derived dermal vascular smooth muscle cells [43]. Therefore, it can be speculated that Tan IIA might have a synergistic or additive therapeutic impact on SSc. Hydrophilic phenolic compounds (like salvianolic acids) and lipophilic diterpenoids (mainly tanshinones) are the main bioactive ingredients found in *S. miltiorrhiza* [44]. The literature indicates that there is a potential synergism *in vivo* among these bioactive constituents [45]. Indeed, another study pointed out that salvianolic acid B could also alleviate SSc-related skin fibrosis [46]. In addition, Tanshinone I can inhibit the proliferation of vascular smooth muscle cells by targeting the PI3K

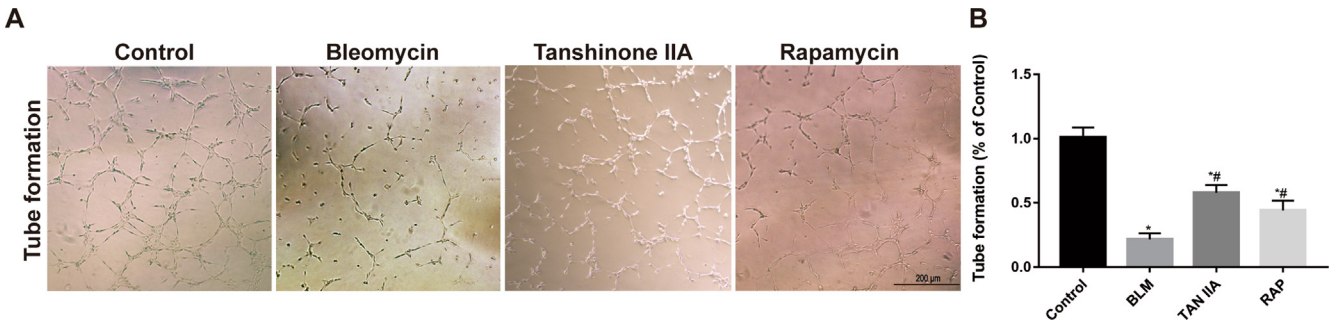

Fig. 3. Tanshinone IIA restored tube formation in HUVECs *in vitro*. HUVECs were seeded in a basement membrane matrix gel and treated with tanshinone IIA, rapamycin, or control dimethylsulfoxide, and then exposed to BLM before tube formation assay using light microscopy (n = 5 independent experiments). Representative images (A) and the quantification of junctions (Image J software) from five randomly selected fields (B) are shown. $^{*}p < 0.05$ compared with the control group; $^{\#}p < 0.05$ compared with the BLM group.

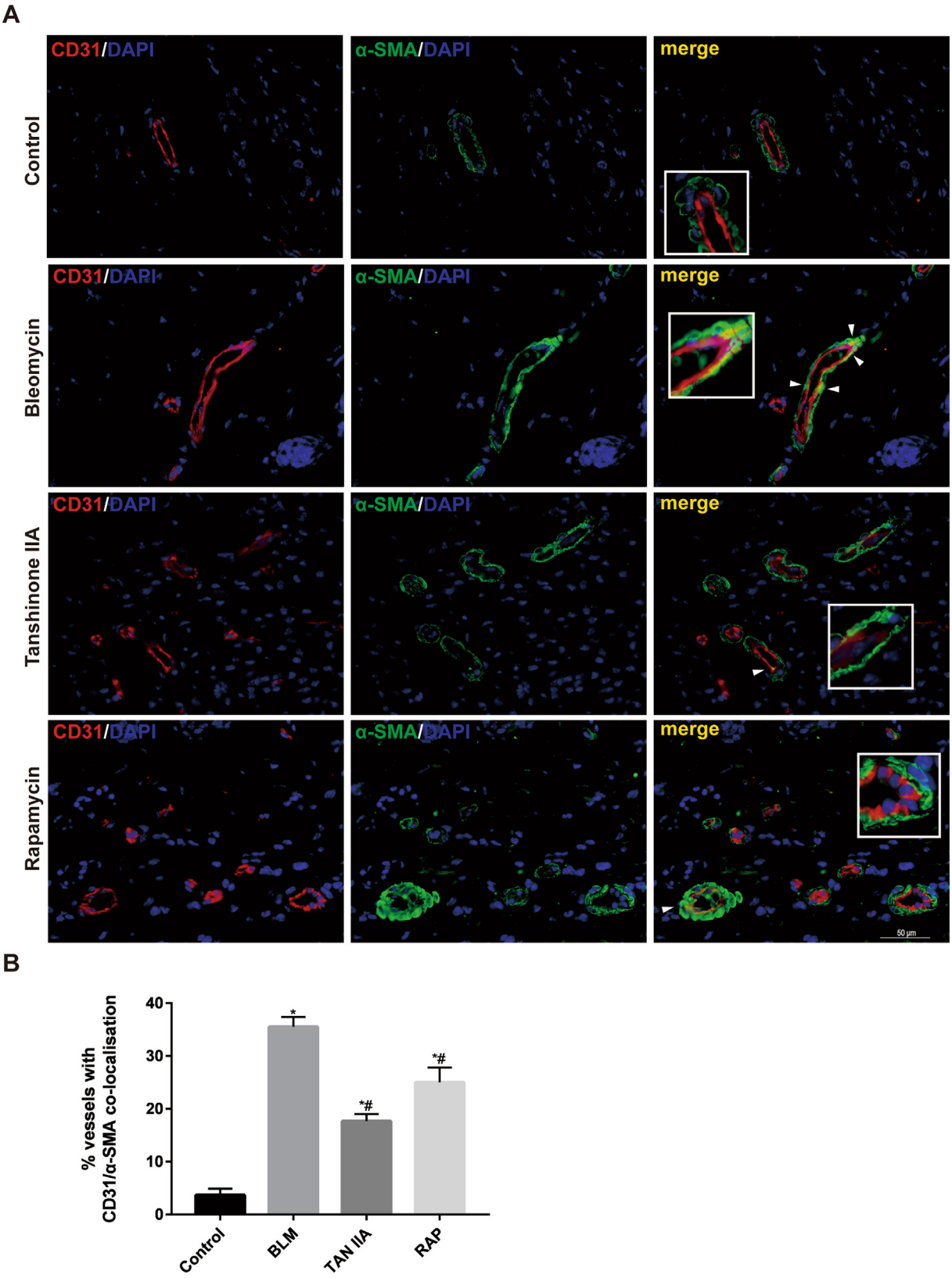

Fig. 4. Tanshinone IIA alleviated the induction of EndoMT in BLM-treated mice. (A) Double immunofluorescence staining of α-SMA (green) and CD31 (red) in skin samples from saline- or BLM-treated mice with the administration of tanshinone IIA or rapamycin. α-SMA/CD31 double-positive cells are indicated with arrows. Insets show higher magnification views of dermal microvessels from the corresponding panels. Scale bar = 50 μm. (B) Data on the dermal vessels displaying CD31/α-SMA co-localization are summarized as a histogram. Each graph indicates mean ± SEM, n = 4. $^{*}p < 0.05$ versus the control group; $^{\#}p < 0.05$ versus the BLM group.

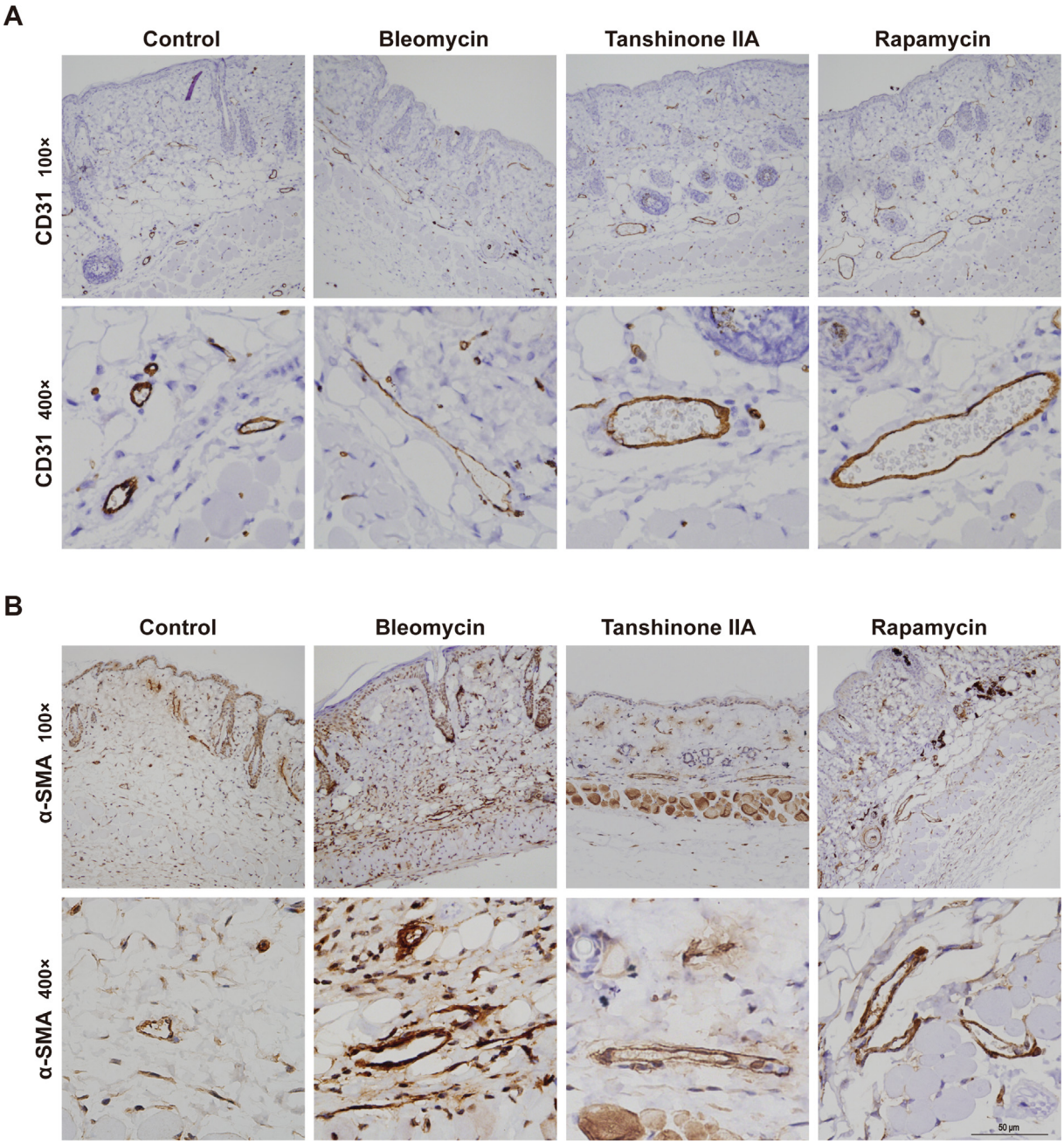

Fig. 5. Distribution and expression of CD31 (A) and α-SMA (B) in the mouse skin tissues were assessed by immunohistochemical staining. Scale bar = 50 μm.

signal pathway [47]. There appears to be some complicated and co-existing cross-talk among these active components of *Salvia miltiorrhiza*, which has been confirmed by recent studies [48].

Although its detailed mechanism still requires further intensive elucidation, we demonstrated that the BLM-induced fibrosis and EndoMT status could be alleviated by Tan IIA, as represented by the downregulation of the level of α-SMA, attenuation of the dermal thickness, reduced collagen content, and co-localized CD31/α-SMA cells. In addition, BLM induced the endothelial cells to undergo this EndoMT-like process through an Akt/mTOR/p70S6K-dependent pathway. Moreover, using a Matrigel model, the endothelial cells' ability to form tubular structures was decreased after incubation with BLM. This reduction could be restored by co-culture with Tan IIA or rapamycin, which indicates the protective effects of Tan IIA under pro-fibrotic conditions. All TGF-β isoforms (1, 2, and 3) can induce EndoMT [10,49], and the mTOR signaling pathway takes part in the TGF-β_1-induced EndoMT [16] and TGF-β_2-induced EMT [17]. Recently, it has been demonstrated that several EndoMT-related transcriptional regulators like Slug and Twist are also significantly upregulated in endothelial cells isolated from the lungs of SSc patients [37]. Consistent with this result, we also found increased levels of Slug and Twist in BLM-induced EndoMT. Furthermore, we demonstrated that the BLM-induced transformation was regulated by Slug in an Akt/mTOR/p70S6K pathway-dependent manner in the SSc mouse model, which was in accordance with an earlier study showing that endothelial cells from SSc lungs express increased genes encoding the EndoMT-related transcription regulators Slug and Twist [8]. Another study elucidated that the nuclear translocation of transcriptional factor Snail1 was the crucial trigger of EndoMT [6,50]. Some reports indicate that over-expression of either Slug or Snail1 could contribute to induce EndoMT, and these differences in transcription factors are activated by diverse dynamic stimuli owing to the local microenvironment [7], which

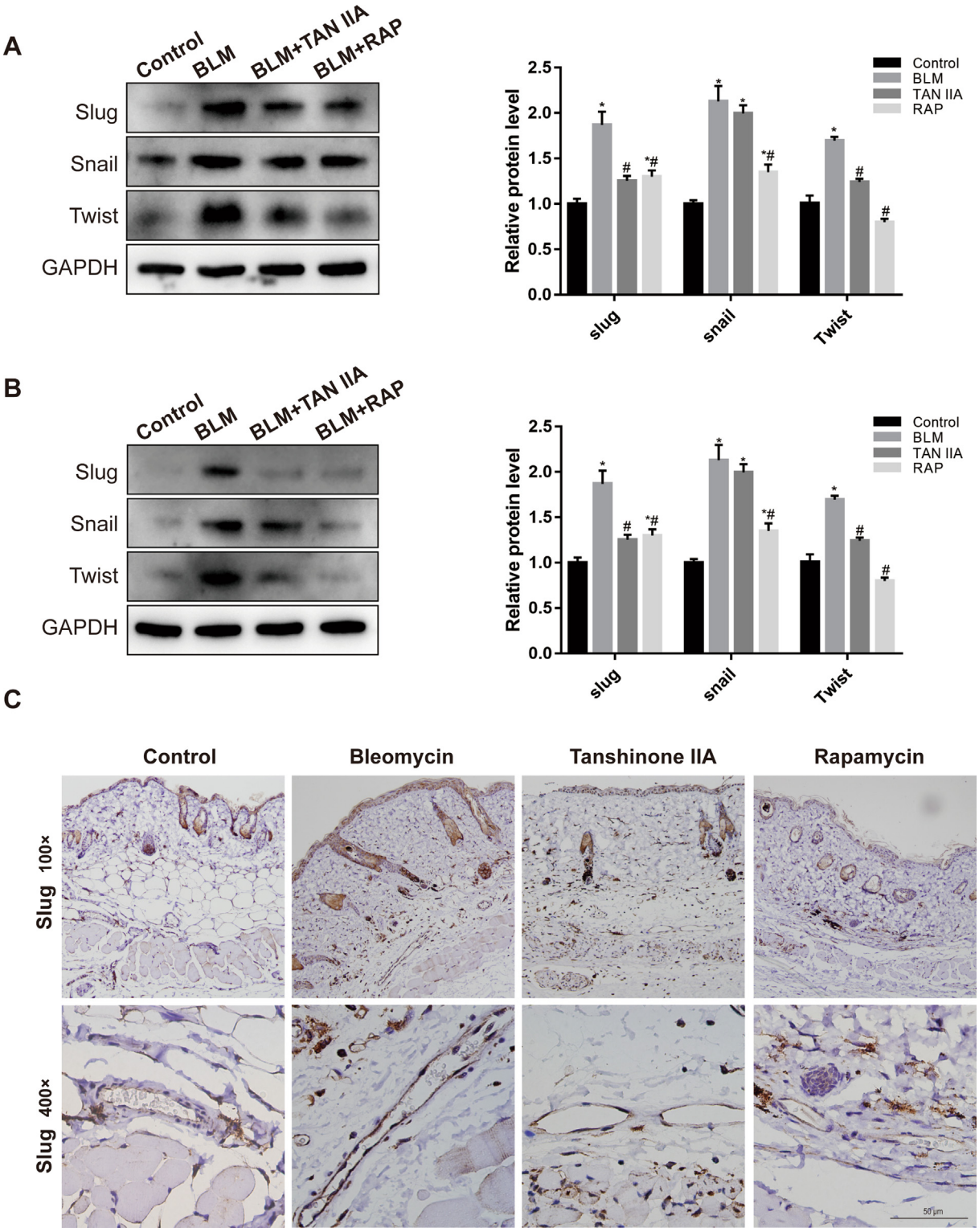

Fig. 6. Tanshinone IIA treatment attenuated the endothelial-to-mesenchymal transition induced by bleomycin. Key factors of the EndoMT (Slug, Snail, and Twist) treated with bleomycin, tanshinone IIA, or rapamycin (positive control) in HUVECs *in vitro* (A) and in the murine model of SSc *in vivo* (B). Western blot analysis and histograms depict the relative protein level in each group. (C) Immunohistochemistry analysis of the key transcription factor Slug. Scale bar = 50 μm. $^{*}p < 0.05$ compared with the control group; $^{\#}p < 0.05$ versus the BLM group.

includes various cytokines, hypoxia, growth factors, and close contact with the surrounding ECM. Nevertheless, the precise mechanisms underlying the intracellular transduction pathways mediating BLM-induced EndoMT remain to be further explored. Our results confirmed that mTOR, as an essential downstream signal of the Akt pathway, participates in EndoMT induced by BLM, which is in accordance with former reports that BLM activates the Akt/mTOR signal pathway and stimulates fibroblasts to synthesize ECM proteins [51].

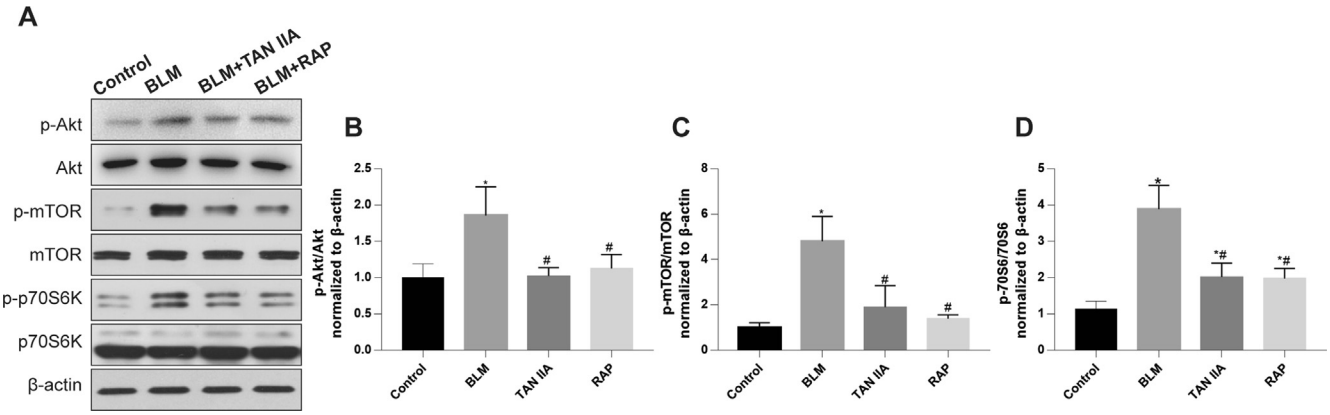

Fig. 7. Effect of Tanshinone IIA on EndoMT through the Akt/mTOR/p70S6K pathway in the SSc mouse model. Western blot analysis (A) and relative protein expression level analyzed by densitometry (B–D) (Image J software). N = 3, $^{*}p < 0.05$ compared with the control group; $^{\#}p < 0.05$ versus the BLM group.

5. Conclusions

In summary, our results provide evidence that the Slug-dependent EndoMT might be involved in the scleroderma mouse model induced by BLM. In addition, the data presented here indicate the potential role of the Akt/mTOR/p70S6K signaling pathway in the therapy of Tan IIA. Therefore, our current findings suggest that Tan IIA has a positive effect on SSc and could be a worthwhile candidate for clinical use.

Disclosure statement

All authors declare that there is no conflict of interest regarding the publication of this article.

Acknowledgment

This work was financially supported by grants from the National Natural Science Foundation of China (81573043, 81803129).

Appendix A. Supplementary material

Supplementary data to this article can be found online at https://doi.org/10.1016/j.intimp.2019.105968.

References

[1] C.P. Denton, D. Khanna, Systemic sclerosis, Lancet 390 (2017) 1685–1699, https://doi.org/10.1016/s0140-6736(17)30933-9.
[2] M. Orlandi, S. Barsotti, G. Lepri, et al., One year in review 2018: systemic sclerosis, Clin. Exp. Rheumatol. 36 (Suppl 113) (2018) 3–23.
[3] Y. Mostmans, M. Cutolo, C. Giddelo, et al., The role of endothelial cells in the vasculopathy of systemic sclerosis: a systematic review, Autoimmun Rev. 16 (2017) 774–786, https://doi.org/10.1016/j.autrev.2017.05.024.
[4] Y. Asano, Systemic sclerosis, J. Dermatol. 45 (2018) 128–138, https://doi.org/10.1111/1346-8138.14153.
[5] Y. Asano, S. Sato, Vasculopathy in scleroderma, Semin. Immunopathol. 37 (2015) 489–500, https://doi.org/10.1007/s00281-015-0505-5.
[6] M. Manetti, E. Romano, I. Rosa, et al., Endothelial-to-mesenchymal transition contributes to endothelial dysfunction and dermal fibrosis in systemic sclerosis, Ann. Rheum. Dis. 76 (2017) 924–934, https://doi.org/10.1136/annrheumdis-2016-210229.
[7] D.M. Gonzalez, D. Medici, Signaling mechanisms of the epithelial-mesenchymal transition, Sci. Signal. 7 (2014) re8, https://doi.org/10.1126/scisignal.2005189.
[8] S.A. Jimenez, Role of endothelial to mesenchymal transition in the pathogenesis of the vascular alterations in systemic sclerosis, ISRN Rheumatol. 2013 (2013) 835948, https://doi.org/10.1155/2013/835948.
[9] L.A. van Meeteren, P. ten Dijke, Regulation of endothelial cell plasticity by TGF-beta, Cell Tissue Res. 347 (2012) 177–186, https://doi.org/10.1007/s00441-011-1222-6.
[10] E. Pardali, G. Sanchez-Duffhues, M.C. Gomez-Puerto, et al., TGF-β-induced endothelial-mesenchymal transition in fibrotic diseases, Int. J. Mol. Sci. 18 (2017) 2157, https://doi.org/10.3390/ijms18102157.
[11] S. Piera-Velazquez, S.A. Jimenez, Molecular mechanisms of endothelial to mesenchymal cell transition (EndoMT) in experimentally induced fibrotic diseases, Fibrogenesis Tissue Repair. 5 (2012) S7, https://doi.org/10.1186/1755-1536-5-s1-s7.
[12] C. Vandewalle, F. Van Roy, G. Berx, The role of the ZEB family of transcription factors in development and disease, CellMol Life Sci. 66 (2009) 773–787, https://doi.org/10.1007/s00018-008-8465-8.
[13] W. Zhang, G. Chen, J.G. Ren, et al., Bleomycin induces endothelial mesenchymal transition through activation of mTOR pathway: a possible mechanism contributing to the sclerotherapy of venous malformations, Br. J. Pharmacol. 170 (2013) 1210–1220, https://doi.org/10.1111/bph.12355.
[14] Y. Cai, R. Sun, R. Wang, et al., The activation of Akt/mTOR pathway by bleomycin in Epithelial-to-mesenchymal transition of human submandibular gland cells: a treatment mechanism of bleomycin for mucoceles of the salivary glands, Biomed. Pharmacother. 90 (2017) 109–115, https://doi.org/10.1016/j.biopha.2017.02.098.
[15] H. Tang, H. He, H. Ji, et al., Tanshinone IIA ameliorates bleomycin-induced pulmonary fibrosis and inhibits transforming growth factor-beta-beta-dependent epithelial to mesenchymal transition, J. Surg. Res. 197 (2015) 167–175, https://doi.org/10.1016/j.jss.2015.02.062.
[16] D. Tian, X. Zeng, W. Wang, et al., Protective effect of rapamycin on endothelial-to-mesenchymal transition in HUVECs through the Notch signaling pathway, Vascul. Pharmacol. 113 (2019) 20–26, https://doi.org/10.1016/j.vph.2018.10.004.
[17] R. Guo, Q. Meng, H. Guo, et al., TGF-beta2 induces epithelial-mesenchymal transition in cultured human lens epithelial cells through activation of the PI3K/Akt/mTOR signaling pathway, Mol. Med. Rep. 13 (2016) 1105–1110, https://doi.org/10.3892/mmr.2015.4645.
[18] J. Xu, K. Wei, G. Zhang, et al., Ethnopharmacology, phytochemistry, and pharmacology of Chinese Salvia species: a review, J. Ethnopharmacol. 225 (2018) 18–30.
[19] W. Chen, X. Li, S. Guo, et al., Tanshinone IIA harmonizes the crosstalk of autophagy and polarization in macrophages via miR-375/KLF4 pathway to attenuate atherosclerosis, Int. Immunopharmacol. 70 (2019) 486–497, https://doi.org/10.1016/j.intimp.2019.02.054.
[20] X. Li, Z. Li, X. Li, et al., Mechanisms of Tanshinone II a inhibits malignant melanoma development through blocking autophagy signal transduction in A375 cell, BMC Can. 17 (2017) 357, https://doi.org/10.1186/s12885-017-3329-y.
[21] G. Gong, Y. Gu, Y. Zhang, et al., Tanshinone IIA alleviates oxidative damage after spinal cord injury in vitro and in vivo through up-regulating miR-124, Life Sci. 216 (2019) 147–155, https://doi.org/10.1016/j.lfs.2018.11.046.
[22] L. Luan, Z. Liang, Tanshinone IIA protects murine chondrogenic ATDC5 cells from lipopolysaccharide-induced inflammatory injury by down-regulating microRNA-203a, Biomed. Pharmacother. 103 (2018) 628–636, https://doi.org/10.1016/j.biopha.2018.04.051.
[23] J. Tang, S. Zhou, F. Zhou, et al., Inhibitory effect of tanshinone IIA on inflammatory response in rheumatoid arthritis through regulating beta-arrestin 2, Exp. Ther. Med. 17 (2019) 3299–3306, https://doi.org/10.3892/etm.2019.7371.
[24] N. Tang, J. Chang, Y. Zeng, et al., Tanshinone IIA protects hypoxia-induced injury by preventing microRNA-28 up-regulation in PC-12 cells, Eur. J. Pharmacol. 854 (2019) 265–271, https://doi.org/10.1016/j.ejphar.2019.04.030.
[25] P. Fu, F. Du, W. Chen, et al., Tanshinone IIA blocks epithelial-mesenchymal transition through HIF-1alpha downregulation, reversing hypoxia-induced chemotherapy resistance in breast cancer cell lines, Oncol. Rep. 31 (2014) 2561–2568, https://doi.org/10.3892/or.2014.3140.
[26] L. Cao, B. Huang, X. Fu, et al., Effects of tanshinone IIA on the regulation of renal proximal tubular fibrosis, Mol. Med. Rep. 15 (2017) 4247–4252, https://doi.org/10.3892/mmr.2017.6498.
[27] L.C. Li, L.D. Kan, Traditional Chinese medicine for pulmonary fibrosis therapy: progress and future prospects, J. Ethnopharmacol. 198 (2017) 45–63, https://doi.org/10.1016/j.jep.2016.12.042.
[28] L. Huang, J. Zhu, M. Zheng, et al., Tanshinone IIA protects against subclinical lipopolysaccharide induced cardiac fibrosis in mice through inhibition of NADPH oxidase, Int. Immunopharmacol. 60 (2018) 59–63, https://doi.org/10.1016/j.intimp.2018.04.036.
[29] M.J. Shi, B.S. Dong, W.N. Yang, et al., Preventive and therapeutic role of

Tanshinone A in hepatology, Biomed. Pharmacother. 112 (2019) 108676, , https://doi.org/10.1016/j.biopha.2019.108676.
[30] D.T. Wang, R.H. Huang, X. Cheng, et al., Tanshinone IIA attenuates renal fibrosis and inflammation via altering expression of TGF-beta/Smad and NF-kappaB signaling pathway in 5/6 nephrectomized rats, Int. Immunopharmacol. 26 (2015) 4–12, https://doi.org/10.1016/j.intimp.2015.02.027.
[31] T. Wu, H. Chu, W. Tu, et al., Dissection of the mechanism of traditional Chinese medical prescription-Yiqihuoxue formula as an effective anti-fibrotic treatment for systemic sclerosis, BMC Complement Altern. Med. 14 (2014) 224, https://doi.org/10.1186/1472-6882-14-224.
[32] C.M. Chang, P.C. Wu, J.H. Chiang, et al., Integrative therapy decreases the risk of lupus nephritis in patients with systemic lupus erythematosus: A population-based retrospective cohort study, J. Ethnopharmacol. 196 (2017) 201–212, https://doi.org/10.1016/j.jep.2016.12.016.
[33] Y.F. Huang, M.L. Liu, M.Q. Dong, et al., Effects of sodium tanshinone II A sulphonate on hypoxic pulmonary hypertension in rats in vivo and on Kv2.1 expression in pulmonary artery smooth muscle cells in vitro, J. Ethnopharmacol. 125 (2009) 436–443, https://doi.org/10.1016/j.jep.2009.07.020.
[34] Q. Qi, Y. Mao, Y. Tian, et al., Geniposide inhibited endothelial-mesenchymal transition via the mTOR signaling pathway in a bleomycin-induced scleroderma mouse model, Am. J. Transl. Res. 9 (2017) 1025–1036.
[35] A. Yoshizaki, K. Yanaba, A. Yoshizaki, et al., Treatment with rapamycin prevents fibrosis in tight-skin and bleomycin-induced mouse models of systemic sclerosis, Arthritis Rheum. 62 (2010) 2476–2487, https://doi.org/10.1002/art.27498.
[36] T. Yamashita, Y. Asano, T. Taniguchi, et al., Glycyrrhizin ameliorates fibrosis, vasculopathy, and inflammation in animal models of systemic sclerosis, J. Invest. Dermatol. 137 (2017) 631–640, https://doi.org/10.1016/j.jid.2016.08.037.
[37] S. Piera-Velazquez, F.A. Mendoza, S.A. Jimenez, Endothelial to mesenchymal transition (EndoMT) in the pathogenesis of human fibrotic diseases, J. Clin. Med. 5 (2016) 45, https://doi.org/10.3390/jcm5040045.
[38] M.T. Lau, P.C. Leung, The PI3K/Akt/mTOR signaling pathway mediates insulin-like growth factor 1-induced E-cadherin down-regulation and cell proliferation in ovarian cancer cells, Can. Lett. 326 (2012) 191–198, https://doi.org/10.1016/j.canlet.2012.08.016.
[39] M. Matucci-Cerinic, B. Kahaleh, F.M. Wigley, Review: evidence that systemic sclerosis is a vascular disease, Arthritis Rheum. 65 (2013) 1953–1962, https://doi.org/10.1002/art.37988.
[40] F.A. Mendoza, S. Piera-Velazquez, J.L. Farber, et al., Endothelial cells expressing endothelial and mesenchymal cell gene products in lung tissue from patients with systemic sclerosis-associated interstitial lung disease, Arthritis Rheumatol. 68 (2016) 210–217, https://doi.org/10.1002/art.39421.
[41] H. Duan, L. Ma, H. Liu, et al., Tanshinone IIA attenuates epithelial-mesenchymal transition to inhibit the tracheal narrowing, J. Surg. Res. 206 (2016) 252–262, https://doi.org/10.1016/j.jss.2016.04.066.
[42] X.H. Niu, H.Y. Hua, W.J. Guo, et al., Clinical efficiency of tanshinone IIA-sulfonate in treatment of liver fibrosis of advanced schistosomiasis, Zhongguo Xue Xi Chong Bing Fang Zhi Za Zhi. 25 (2013) 137–140.
[43] M. Liu, J. Yang, M. Li, Tanshinone IIA attenuates interleukin-17A-induced systemic sclerosis patient-derived dermal vascular smooth muscle cell activation via inhibition of the extracellular signal-regulated kinase signaling pathway, Clinics (Sao Paulo) 70 (2015) 250–256, https://doi.org/10.6061/clinics/2015(04)06.
[44] A. Contreras, B. Leroy, P.A. Mariage, et al., Proteomic analysis reveals novel insights into tanshinones biosynthesis in Salvia miltiorrhiza hairy roots, Sci. Rep. 9 (2019) 5768, https://doi.org/10.1038/s41598-019-42164-3.
[45] Z.M. Li, S.W. Xu, P.Q. Liu, Salvia miltiorrhizaBurge (Danshen): a golden herbal medicine in cardiovascular therapeutics, Acta Pharmacol. Sin. 39 (2018) 802–824, https://doi.org/10.1038/aps.2017.193.
[46] Q. Liu, J. Lu, J. Lin, et al., Salvianolic acid B attenuates experimental skin fibrosis of systemic sclerosis, Biomed. Pharmacother. 110 (2019) 546–553, https://doi.org/10.1016/j.biopha.2018.12.016.
[47] Y.T. Wu, Y.M. Bi, Z.B. Tan, et al., Tanshinone I inhibits vascular smooth muscle cell proliferation by targeting insulin-like growth factor-1 receptor/phosphatidylinositol-3-kinase signaling pathway, Eur. J. Pharmacol. 853 (2019) 93–102, https://doi.org/10.1016/j.ejphar.2019.03.021.
[48] Z. Wang, S. Fei, C. Suo, et al., Antifibrotic effects of hepatocyte growth factor on endothelial-to-mesenchymal transition via transforming growth factor-beta1 (TGF-beta1)/Smad and Akt/mTOR/P70S6K signaling pathways, Ann. Transplant. 23 (2018) 1–10.
[49] S. Milani, H. Herbst, D. Schuppan, et al., Transforming growth factors beta 1 and beta 2 are differentially expressed in fibrotic liver disease, Am. J. Pathol. 139 (1991) 1221–1229.
[50] M.T. Pinto, F.U. Ferreira Melo, T.M. Malta, et al., Endothelial cells from different anatomical origin have distinct responses during SNAIL/TGF-beta2-mediated endothelial-mesenchymal transition, Am. J. Transl. Res. 10 (2018) 4065–4081.
[51] A. Goc, M. Choudhary, T.V. Byzova, et al., TGFbeta- and bleomycin-induced extracellular matrix synthesis is mediated through Akt and mammalian target of rapamycin (mTOR), J. Cell Physiol. 226 (2011) 3004–3013, https://doi.org/10.1002/jcp.22648.